



# The X-ray binary populations of M81 and M82

Paul H. Sell<sup>1,2</sup> , Andreas Zezas<sup>1,2</sup>, Stephen J. Williams<sup>1,2</sup>,  
Jeff J. Andrews<sup>1,2</sup> , Kosmas Gazeas<sup>3</sup>, John S. Gallagher<sup>4</sup>  
and Andrew Ptak<sup>5</sup>

<sup>1</sup>Department of Physics, University of Crete, Heraklion, Greece  
email: [psell@physics.uoc.gr](mailto:psell@physics.uoc.gr)

<sup>2</sup> Foundation for Research and Technology Hellas (FORTH), Heraklion, Greece

<sup>3</sup> Department of Astrophysics, University of Athens, Zografos, Athens, Greece

<sup>4</sup> Department of Astronomy, University of Wisconsin-Madison, Madison, WI, USA

<sup>5</sup> NASA Goddard Space Flight Center, Code 662, Greenbelt, MD 20771, USA

**Abstract.** We use deep Chandra and HST data to uniquely classify the X-ray binary (XRB) populations in M81 on the basis of their donor stars and local stellar populations (into early-type main sequence, yellow giant, supergiant, low-mass, and globular cluster). First, we find that more massive, redder, and denser globular clusters are more likely to be associated with XRBs. Second, we find that the high-mass XRBs (HMXBs) overall have a steeper X-ray luminosity function (XLF) than the canonical star-forming galaxy XLF, though there is some evidence of variations in the slopes of the sub-populations. On the other hand, the XLF of the prototypical starburst M82 is described by the canonical powerlaw ( $\alpha_{\text{cum}} \sim 0.6$ ) down to  $L_X \sim 10^{36}$  erg s<sup>-1</sup>. We attribute variations in XLF slopes to different mass transfer modes (Roche-lobe overflow versus wind-fed systems).

**Keywords.** accretion, stars: neutron, galaxies: star clusters, galaxies: individual (M81, M82), galaxies: spiral, galaxies: starburst, X-rays: binaries

---

## 1. Introduction

X-ray observations of star-forming galaxies reveal abundant point sources that dominate the galaxies' hard X-ray emission. Most of these sources are XRBs with a neutron star or black hole accreting matter from a high- or low-mass stellar companion through Roche lobe overflow or stellar winds. XRBs are an important evolutionary stage in binary stellar systems, occurring after one star has undergone a supernova, formed a compact object, and then brought it into contact with the other star (e.g., [Tauris & van den Heuvel 2010](#)).

XRBs have important links to various topics in astrophysics: they are responsible for feedback (winds, jets, and ionization) on multiple scales (e.g., [Soria et al. 2010](#); [Justham & Schawinski 2012](#)) including preheating the intergalactic medium prior to and during reionization ([Fragos et al. 2013](#); [Das et al. 2017](#); [Douna et al. 2018](#)) and they are prime candidates for progenitors of gravitational wave events ([Abbott et al. 2016](#)).

Observations of elliptical galaxies and bulges of spirals in nearby galaxies enable us to isolate the low-mass XRB (LMXB) populations of galaxies (e.g., [Kong et al. 2003](#); [Kim & Fabbiano 2010](#)) and study trends with stellar mass across many LMXB populations ( $M_*$ ; [Boroson et al. 2011](#); [Zhang et al. 2011](#)). Similar work has been done with nearby star-forming galaxies to locate HMXBs (e.g., [Zezas et al. 2002](#); [Pannuti et al. 2011](#)) and study their links to the recent star formation rate (SFR; [Mineo et al. 2012](#); [Mineo et al. 2014](#)).

Regions containing HMXBs are usually mixed with other populations of sources: notably LMXBs but also supernova remnants (SNRs; Leonidaki *et al.* 2010) and hyper-accreting white dwarfs frequently seen as super-soft sources (SSSs; e.g., Di Stefano & Kong 2004). Only in rare cases with very high specific SFR ( $sSFR=SFR/M_*$ ) or where individual counterparts are identified can we examine these populations with very low contamination: the Milky Way (Grimm *et al.* 2002) though heavily biased (Arur & Maccarone 2018), SMC/LMC (Antoniou *et al.* 2009; Antoniou & Zezas 2016), M33 (Tüllmann *et al.* 2011; Garofali *et al.* 2018), and M31 (Lazzarini *et al.* 2018). We extend this work to two more nearby interacting galaxies: M81 and M82.

## 2. Source Classification in M81

The primary goal of our work on M81 is to carefully identify and study the LMXB and HMXB source populations. We briefly outline our approach using the best optical and X-ray observations of the galaxy.

For all Chandra sources, we construct 3-color stamps of the local HST stellar fields and their corresponding color-magnitude diagrams (CMDs; where necessary). We first identify interlopers (class “A” in Fig. 1): foreground stars (identified on the basis of their brightness on the HST images and their soft X-ray colors), and background galaxies (clearly seen on the HST images). Another of these categories are X-ray sources associated with clusters (identified in the basis of their spatial extent on the HST images and their location on the CMD). X-ray sources associated with globular clusters are, by definition, LMXBs (class “B” in Fig. 1). Finally, using a combination of X-ray colors and optical spectroscopic line diagnostics, we have discovered a population of SNRs (Leonidaki *et al.* in prep.).

For all the other sources, we follow a systematic approach for X-ray source classification based on the location of their optical associations on the CMD and their corresponding chance coincidence probability (CCP). This is determined by randomly shifting the Chandra and HST catalogs and calculating the likelihood that an X-ray source will match an HST source of the corresponding location on the CMD. The CCP is simply a ratio of the number of matched HST sources of a certain type (location on the CMD) to the total number of tries and is a function of the search radius and local stellar density. Therefore, it is normalized probability, where very small CCPs ( $\sim 0$ ) refer to very rare sources and large CCPs ( $\sim 1$ ) refer to chance associations. Extremely rare sources are more likely to be matched to their true counterparts. This procedure of matching by exclusion has been very commonly used to match source catalogs (see e.g., Antoniou *et al.* 2009 for a more detailed description of the CCP).

The search radius for each X-ray source depends on its off axis angle and number of counts. We use the prescription of Hong *et al.* (2005), which is based on extensive simulations. The full position probability at an arbitrary radius is calculated as a quadrature sum between the boresight uncertainty ( $\delta_{RA,Dec} \sim 0.1''$ ) between the catalogs and the reported 95% confidence in Hong *et al.* modeled as a symmetric Gaussian. We consider all HST sources within the  $3\sigma$  position error circle, which ensures that we are not missing the true counterpart.

We compare all HST sources in the X-ray error circle by assigning weights based on their chance coincidence probability. A full description of the calculation of the CCP, the weights, and their application to the source matching will be presented in a follow-up publication (Sell *et al.* in prep.). Examples of the HMXB and field LMXB sources in each of our remaining categories are shown in Fig. 1 (classes “C–F”). Some sources are excluded, as their classifications are ambiguous (class “G”). In Fig. 2, we present on the CMD each Chandra source with a unique/clear high-mass star counterpart.

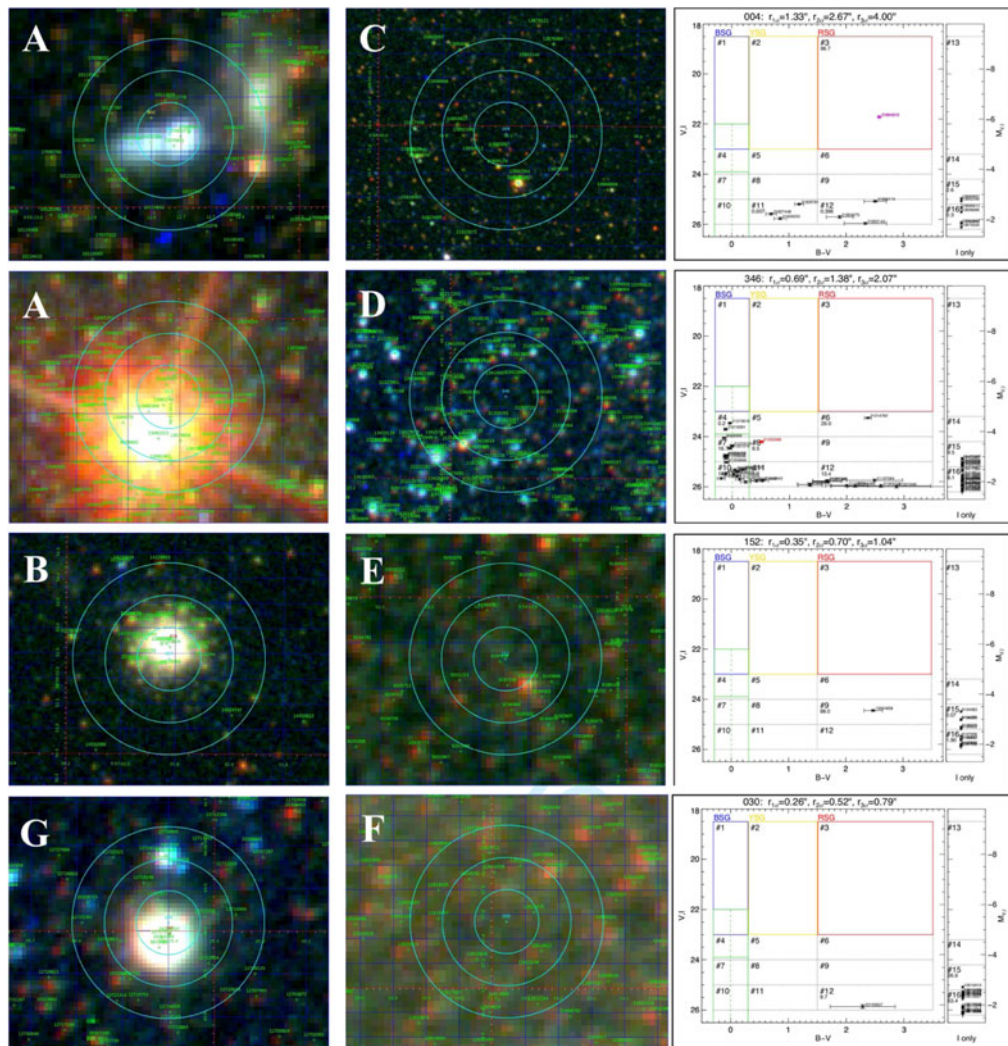


**Figure 1.** We show examples of various source classification categories using 3-color (B, V, and I) stamps of HST fields local to each Chandra source with observational color-magnitude diagrams when relevant: A) interlopers (background galaxies and foreground stars), B) LMXBs in globular clusters, C) uniquely classified HMXBs, D) confused HMXBs, E) uniquely classified LMXBs, F) confused LMXBs (e.g. extremely high stellar density in the bulge; only faint, low-mass stars in the field) and G) indeterminate sources, (likely either a low- or high-mass star). In the stamps, the  $1\sigma$ ,  $2\sigma$ , and  $3\sigma$  Chandra astrometric error circles are shown in cyan, the HST catalog sources with their ID numbers are in green, and the globular clusters and galaxies are in red and yellow, respectively. We construct each CMD using the observed B, V and I magnitudes of the stars within  $3\sigma$ , identified by their HST source ID numbers. Each left plot includes sources with matches in all three bands and each right plot includes sources only present in the I-band. The Chandra source number and its  $1\sigma$ ,  $2\sigma$ , and  $3\sigma$  astrometric uncertainties are listed in the plot title and physically-motivated (blue, yellow and red supergiants, main-sequence stars—green) regions where we have calculated the chance coincidence are numbered. The CMD weight is below the CMD#.

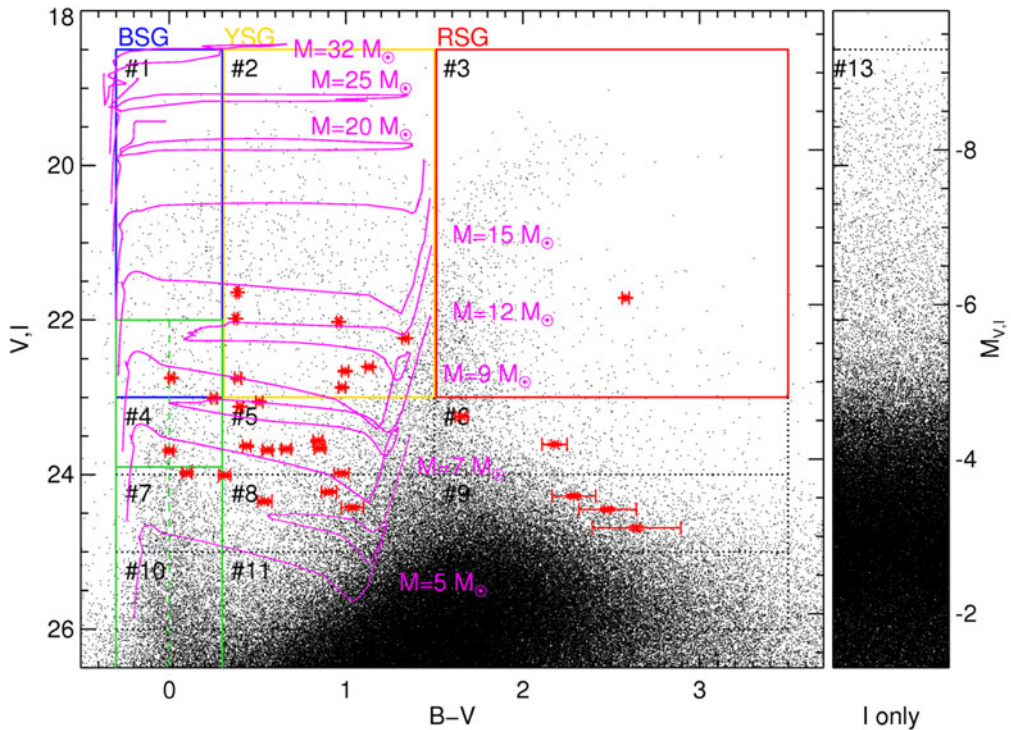


**Figure 2.** The CMD for all Chandra sources with unique HST counterparts (red). The black dots indicate all HST sources within  $5''$  of each of the sources in our X-ray catalog. Geneva single star tracks are overplotted for reference (Ekstrom *et al.* 2012).

### 3. Results

#### 3.1. Low-Mass X-ray Binaries in M81 Globular Clusters

We examine the optical properties of the M81 globular cluster population, including those with XRBs (Fig. 3). We find that XRBs are preferentially associated with redder, more massive, and denser clusters in agreement with other work on elliptical galaxies (e.g., Sivakoff *et al.* 2007). The similarity between spiral and elliptical galaxies suggests that the same dynamical mechanisms are involved in the formation of LMXBs in GCs in both types of galaxies.

#### 3.2. X-ray Luminosity Functions of M81 and M82

We examine the global properties of the X-ray point source populations of M81 and M82 through their XLFs (Fig. 4). For M81, use the X-ray luminosities from Sell *et al.* (2011). For M82, we use a very similar approach to Sell *et al.* (2011) for calculating source luminosities based on spectral fits that will be discussed in detail in a future publication (Sell *et al.* in prep.).

First for M81, our source-by-source classification enables us to uniquely examine XLFs of different subpopulations (Fig. 4). When there is some uncertainty in our classifications (i.e., an X-ray source has more than one optical association with comparable CCP), we draw sources into the XLFs relative to their CCPs. This is indicated by the scatter in each of the global LMXB (red) and HMXB (blue) populations in Fig. 4 (we only show one realization in the other cases for clarity). The LMXB XLF shows the typical break near  $L_X \sim 10^{38}$  erg s $^{-1}$  (e.g., Fabbiano 2006). Interestingly, we find that the HMXB XLF

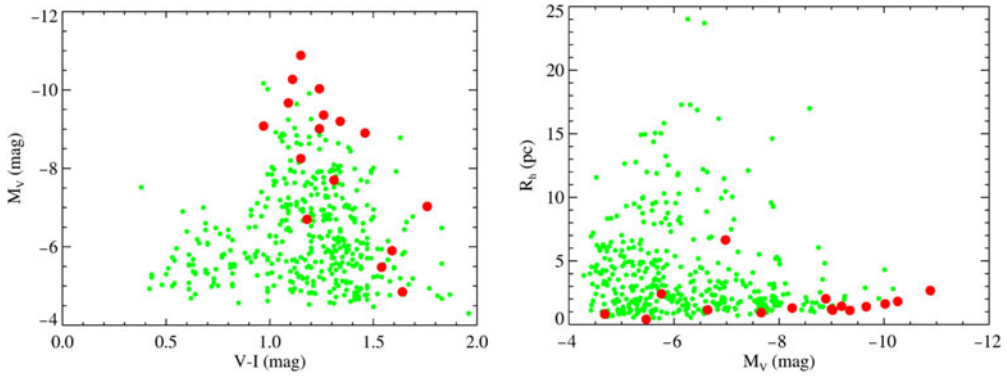


**Figure 3.** Above we plot the observed CMD and the effective radius versus absolute V-band magnitude for the entire M81 globular cluster population (green; *Nantais et al. 2011*) and those with LMXBs (red).

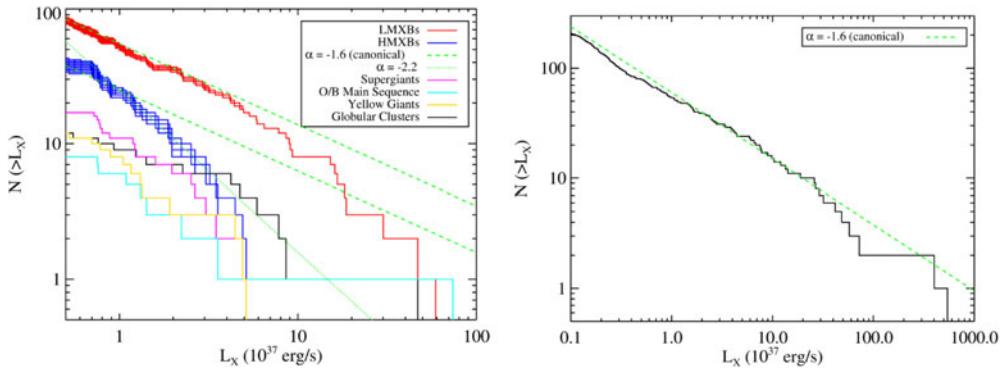


**Figure 4. Left:** XLFs for individually classified XRBs in M81 (incompleteness is important for  $L_X \lesssim 10^{37} \text{ erg s}^{-1}$ ). **Right:** The XLF for M82, the deepest for a starburst galaxy. Unusually high levels of copious diffuse emission account for some incompleteness seen for  $L_X \lesssim 10^{37} \text{ erg s}^{-1}$ . In both plots, the canonical HMXB XLF ( $dN/dL \propto L^\alpha$ ; *Mineo et al. 2012*) is overplotted in green dashed lines.

appears steeper than the canonical HMXB XLF (the green dashed line; *Mineo et al. 2012*, which may include some contamination from LMXBs). The differences in HMXB slopes could be attributed to differences in the mass transfer mode (Roche-lobe overflow vs. wind-fed systems) in the XRB populations comprising each XLF.

We compare these results with the XRB populations of the prototypical starburst galaxy, M82, for which we present one of the deepest XLFs reported for a starburst galaxy. We find that it is described by the canonical powerlaw with a cumulative slope of  $\sim 0.6$  (*Mineo et al. 2012*) down to  $L_X \sim 10^{36} \text{ erg s}^{-1}$ .

### Acknowledgments

The research leading to these results has received funding from the European Research Council under the European Union’s Seventh Framework Programme (FP/2007-2013) / ERC Grant Agreement n. 617001. This project has received funding from the European Union’s Horizon 2020 research and innovation programme under the Marie Skłodowska-Curie RISE action, grant agreement No 691164 (ASTROSTAT).

## References

- Abbott, B. P., *et al.* 2016, *Phys. Rev. Lett.*, 116, 1102
- Antoniou, V., Zezas, A., Hatzidimitriou, D., McDowell, J. C. 2009, *ApJ*, 697, 1695
- Antoniou, V. & Zezas, A. 2016, *MNRAS*, 459, 528
- Arur K. & Maccarone, T. J. 2018, *MNRAS*, 474, 69
- Boroson, B., Kim, D.-W., Fabbiano, G. 2011, *ApJ*, 729, 12
- Das, A., Mesinger, A., Pallottini, A., Ferrara, A., & Wise, J. H. 2017, *MNRAS*, 469, 1166
- Di Stefano, R. & Kong, A. K. H. 2004, *ApJ*, 609, 710
- Douna, V. M., Pellizza, L. J., Laurent, P., & Mirabel, I. F. 2018, *MNRAS*, 474, 3488
- Ekström, S., Georgy, C., Eggenberger, P., Meynet, G., Mowlavi, N., Wyttenbach, A., Granada, A., Decressin, T., Hirschi, R., Frischknecht, U., Charbonnel, C., & Maeder, A. 2012, *A&A*, 537, A146
- Fabbiano, G. 2006, *ARAA*, 44, 323
- Fragos, T., Lehmer, B. D., Naoz, S., Zezas, A., & Basu-Zych, A. 2013, *ApJ*, 776, L31
- Garofali, K., Williams, B. F., Hillis, T., Gilbert, K. M., Dolphin, A. E., Eracleous, M., Binder, B. 2018, *MNRAS*, 479, 3526
- Grimm, H.-J., Gilfanov, M., & Sunyaev, R. 2002, *A&A*, 391, 923
- Hong, J., van den Berg, M., Schlegel, E. M., Grindlay, J. E., Koenig, X., Laycock, S., & Zhao, P. 2005, *ApJ*, 635, 907
- Justham, S. & Schawinski, K. 2012, *MNRAS*, 423, 1641
- Kim, D.-W., & Fabbiano, G. 2010, *ApJ*, 721, 1523
- Kong, A. K. H., DiStefano, R., Garcia, M. R., & Greiner, J. 2003, *ApJ*, 585, 298
- Lazzarini, M., Hornschemeier, A. E., Williams, B. F., Wik, D., Vulic, N., Yukita, M., Zezas, A., Lewis, A. R., Durbin, M., Ptak, A., Bodaghee, A., Lehmer, B. D., Antoniou, V., & Maccarone, T. 2018, *ApJ*, 862, 28
- Leonidaki, I., Zezas, A., & Boumis, P. 2010, *ApJ*, 725, 842
- Mineo, S., Gilfanov, M., & Sunyaev, R. 2012, *MNRAS*, 419, 25
- Mineo, S., Gilfanov, M., Lehmer, B. D., Morrison, G. E., & Sunyaev, R. 2014, *MNRAS*, 437, 1698
- Nantais, J. B., Huchra, J. P., Zezas, A., Gazeas, K., & Strader, J. 2011, *AJ*, 142, 183
- Pannuti, T. G., Schlegel, E. M., Filipović, M. D., Payne, J. L., Petre, R., Harrus, I. M., Staggs, W. D., & Lacey, C. K. 2011, *AJ*, 142, 20
- Sell, P. H., Pooley, D., Zezas, A., Heinz, S. Homan, J., & Lewin, W. H. G. 2011, *ApJ*, 735, 26
- Sivakoff, G. R., Jordán, A., Sarazin, C. L., Blakeslee, J. P., Côté, P., Ferrarese, L., Juett, A. M., Mei, S., & Peng, E. W. 2007, *ApJ*, 660, 1246
- Soria, R., Pakull, M. W., Broderick, J. W., Corbel, S., Motch, C. 2010, *MNRAS*, 409, 541
- Tüllmann, R., Gaetz, T. J., Plucinsky, P. P., Kuntz, K. D., Williams, B. F., Pietsch, W., Haberl, F., Long, K. S., Blair, W. P., Sasaki, M., Winkler, P. F., Challis, P., Pannuti, T. G., Edgar, R. J., Helfand, D. J., Hughes, J. P., Kirshner, R. P., Mazeh, T., & Shporer, A. 2011, *ApJS*, 193, 31
- Tauris, T. M. & van den Heuvel, E. P. J. 2010, *Compact Stellar X-ray Sources*, 623
- Zezas, A., Fabbiano, G., Rots, A. H., & Murray, S. S. 2002, *ApJ*, 577, 710
- Zhang, Z., Gilfanov, M., Voss, R., Sivakoff, G. R., Kraft, R. P., Brassington, N. J., Kundu, A., Jordán, A., Sarazin, C. 2011, *A&A*, 533, 33